Trace element and organic matter mobility impacted by Fe 3 O 4 -nanoparticle surface coating within wetland soil

Maya Al-Sid-Cheikh, Mathieu Pédrot, Aline N. Dia, Mélanie Davranche, Laurent Jeanneau, Patrice Petitjean, Martine Bouhnik-Le Coz, Marc-André Cormier, Fabien Grasset

Environmental Science Nano

Trace element and organic matter mobility impacted by Fe3O4-nanoparticles surface coating within wetland soil

Journal:	*Environmental Science: Nano*
Manuscript ID	Draft
Article Type:	Paper
Date Submitted by the Author:	n/a
Complete List of Authors:	Al-Sid-Cheikh, Maya; University of Rennes1, Geosciences Pedrot, Mathieu; Rennes 1 University, Geosciences Dia, Aline; Rennes 1 University, Geosciences Davranche, Mélanie; Rennes 1 University, Geosciences Jeanneau, Laurent; Rennes 1 University, Geosciences Petitjean, Patrice; Rennes 1 University, Geosciences Bouhnik-Le-Coz, Martine; Universite de Rennes 1, Geosciences Cormier, Marc-André; ETH Zürich, Heart Sciences Grasset, Fabien; CNRS-Saint-Gobain-NIMS UMI LINK 3629

Environmental statement

"**Trace element and organic matter mobility impacted by Fe_3O_4-nanoparticles surface coating within wetland soil**" by Maya Al-Sid-Cheikh, Mathieu Pédrot, Aline Dia, Mélanie Davranche, Laurent Jeanneau, Patrice Petitjean, Martine Bouhnik-Le Coz, Marc-André Cormier, and Fabien Grasset

Most studies investigating iron oxide nanoparticles to remediate soils from pollutants have employed artificial porous materials, overlooking many soil properties and questioning their relevance to fully understand the transport dynamic of iron oxide nanoparticles in natural settings. We investigated the impact of uncoated and coated magnetite nanoparticles on the mobility of TEs and SOM within leaching experiments on a natural wetland soil. While our study is the first to show different impacts of two nanoparticle surfaces on the behaviour of the SOM and TEs in a natural system, we also evidenced that the nFe3O4 surface composition has an impact on the TEs mobility and could also be involved in a transfer of TEs into deeper soil horizon or groundwater.

ARTICLE

Trace element and organic matter mobility impacted by Fe_3O_4-nanoparticles surface coating within wetland soil

Received 00th January 20xx,
Accepted 00th January 20xx

DOI: 10.1039/x0xx00000x

www.rsc.org/

Maya Al-Sid-Cheikh[†*a], Mathieu Pédrot[a], Aline Dia[a], Mélanie Davranche[a], Laurent Jeanneau[a], Patrice Petitjean[a], Martine Bouhnik-Le Coz[a], Marc-André Cormier[b,c], and Fabien Grasset[d,e]

Engineered oxide nanoparticles have appeared as a highly promising tool for soil remediation. However, their behaviour under complex environmental exposures (i.e. in natural soils) remains poorly understood and a relevant issue to complete their risk assessments. Prior using iron oxide nanoparticles in soil remediation scenarios, it is crucial to evaluate their possible role on the release of natural organic matter (NOM) and trace elements (TEs) as a vector of trace elements (TEs) as it could contribute to the contamination of aquifers. This work presents leaching experiments demonstrating the effects of magnetite (i.e. nFe_3O_4) on TEs and natural organic matter (NOM) transport within an organo-mineral horizon from a natural wetland. nFe_3O_4 (~10nm) with two different surface compositions (i.e. uncoated and dimercapto-succinic acid (DMSA) coating) were used in the experiments and both forms impacted the mobility of the NOM within the organo-mineral horizon. The mobility of the coated nFe_3O_4 within the horizon was higher than the uncoated nFe_3O_4 and impacted differently the mobility of TEs and NOM. TEs mobility within the horizon increased in presence of uncoated nFe_3O_4 with a transfer of elements into the colloidal fraction. This distinctive transfer might be explained by interactions between the surface of nanoparticles with NOM. We also suggest that some of the different behaviours observed might be due to the destabilization of the DMSA coating, highlighting the critical importance of understanding the aging processes of nanoparticles under environmental exposures to assess the risks associated with their use in environmental situations.

Introduction

The increasing production of various engineered nanoparticles (ENPs) and their widespread utilization will inevitably result in their release into the environment[1–3]. The environmental fate and behaviour of ENPs were thus extensively studied over the last decade. As such, several studies have pointed out diverse biological effects associated with various ENPs[1,4,5]. Nano-sized metal oxides (<100 nm) such as iron oxides provide high surface area and specific affinity for heavy metals and metalloids such as As in aqueous systems[6]. This has raised concerns about their potential to have indirect toxic effects as inorganic pollutant carriers[7]. For instance, the magnetic iron nanoparticles (i.e. nFe_3O_4, $n\gamma Fe_2O_3$) attracted much attention for their apparent capacity to trap and remove toxic metals and metalloids from polluted area (e.g. [8,9]). It is expected that this advantageous property will promote their use, for example, in soil remediation scenarios[6,10]. Understanding their behaviour and interactions with heavy metals in soils under realistic conditions is therefore essential as their ill-advised utilization could instead contribute to the contamination of aquifers.

The first efforts to understand the behaviour of ENPs in soils focused on transport mechanisms in porous media. As such, several leaching studies have shown that alongside their surface properties (i.e. surface charge and coating), ENPs mobility in porous media is strongly dependent on soil textural properties (i.e. the pore size distribution and pores structure) and physicochemical parameters (i.e. ionic strength, pH, presence of natural organic matter, etc.)[11]. However, most of the studies used artificial porous media with well-defined material such as glass beads[12], homogeneous quartz[13,14] or sand in column experiments[11,15,16]. Only a few studies investigated the transport of ENPs in natural soils. For instance, the works of Sagee et al.[17] carried out using a Mediterranean sandy clay soil pointed out the importance of humic acids in the transport of

[a] Univ Rennes, CNRS, Géosciences Rennes - UMR 6118 F - 35042 Rennes, France
[b] Department of Earth Science, Geological Institute, Climate Geology, ETH Zürich, Sonnegstrasse, Zürich, Switzerland
[c] University of Oxford, Department of Earth Sciences, Ocean Biogeochemistry Group, South Parks road, Oxford, OX1 3AN, United Kingdom
[d] Univ Rennes, CNRS, ISCR (Institut des Sciences Chimiques de Rennes), UMR 6226 – F-35000 Rennes, France
[e] CNRS-Saint Gobain-NIMS, Laboratory for Innovative Key Materials and Structures, UMI3629 LINK, National Institute of Material Science, 1-1 Namiki, 305-0044, Tsukuba, Japan
† Present address, School of Biology and Marine Sciences, Plymouth University, Drake Circus, Plymouth, PL4 8AA, United Kingdom.
Electronic Supplementary Information (ESI) available: A PDF file is available with: key properties of soil grain size mixtures, initial composition of the leaching solution for three exposures, mass balance and percentage of organic carbon and iron for fraction below 0.22µm, dissolved organic carbon and total iron values for fractionation samples with S1, S2, S4, S8 and S12 during all leaching, trace elements analysis on nF_3O_4 uncoated and coated, TEM images and pH_{zpc} of all nFe_3O_4, XRD images, study site localization, illustration of the three elements behaviour (i.e. Sr, Cu and U) during the leaching and SUVA and Aromaticity treatment, procedure and data treatment for Py-GCMS analysis. See DOI: 10.1039/x0xx00000x

ENPs. Other studies have highlighted the role of natural organic matter (NOM) in the mobility of several trace elements (TEs) in soils (e.g. Al-Wabel et al.[18]; Langner et al.[19,20]). This is consistent with field observations, where a large fraction of TEs is indeed closely associated to NOM and to the colloidal fraction in many natural waters and soils[21]. Unfortunately, as artificial porous media do not exemplify the complete soil complexity, most of the studies cannot really evaluate the possible role of ENPs as a vector of TEs in soils.

An important part of the soil complexity lies on the presence of natural organic and inorganic colloids, which can interact with many elements and thus play a key role in their mobilization. Many TEs can adsorb onto organic-rich colloidal material (i.e. NOM), which can then be sequestrated into the soil forming organo-mineral complex or transferred into ground and surface waters with NOM[22]. For example, it has been shown that radionuclides can be transported to groundwaters by the soil colloids[23]. Also, a strong correlation between organic matter and many transition elements, including Co, Ni, Cu, Pb and Zn has been shown (e.g.[21,24]). Natural iron colloids such as iron oxy-hydroxides have also been shown to carry several TEs including As, Ba, Co, Cr, Cu, Ni, Pb and Zn[25]. While nFe_3O_4 have shown a great adsorption capacity of TEs, their impact on TEs mobility in natural systems, where the presence of natural organic and inorganic colloids also contributes, remains unknown. Considering the natural role of natural iron oxide colloids on TEs mobility, the high reactivity of nanoparticles, and their potential to outcompete carbon material to adsorb TEs[26], it is critical to understand the fate of nFe_3O_4 in natural soils to complete their risk assessment.

The aim of the present study was to investigate the effect of nFe_3O_4 on the mobility of TEs, organic and inorganic colloids in natural soils. Column leaching experiments were thus carried out using a natural soil from a riparian wetland chosen for its high TEs and NOM concentrations as well as for its key role in aquatic environmental systems. Uncoated and dimercapto-succinic acid (DMSA)-coated nFe_3O_4s were used. The leaching solutions were analysed by spectrophotometry (for aromaticity), pyrolysis gas-chromatography mass spectrometry (Py-GCMS; for NOM characterization) and inductively coupled plasma mass spectrometry (ICP-MS; for total element concentrations in filtrated and ultrafiltrate fractions). Finally, the soil columns were analysed by micro X-ray fluorescence (µXRF) after the experiments to determine the ENPs distributions within the soil column.

Experimental

Synthesis of nFe_3O_4

Uncoated iron oxide nanoparticles (i.e. nFe_3O_4) were prepared using the Massart's method[27] according to Duguet et al.[28]. These preparations include soft chemistry using co-precipitation of the precursor cations $FeSO_4{\cdot}4H_2O$ (99 %, Aldrich) and $Fe(NO_3)_3{\cdot}6H_2O$ (99 %, Acros) (Fe^{2+}/Fe^{3+} = 1/2) in distilled water. The mixture was dropped into 200 mL of NaOH solution (2 mol L^{-1}) under vigorous stirring for about 30 min. A black precipitate of magnetite was formed. The precipitate was isolated by decantation on a magnet, separated by centrifugation (4000 rpm), washed in acetone, and dispersed in pure water. The nFe_3O_4 washing step was repeated three times. The nFe_3O_4s were kept in water solution and stored in a gloves box under nitrogen atmosphere to avoid oxidation. nFe_3O_4 characterizations (i.e. Transmission Electronic Microscopy (TEM), electronic diffraction image, trace elements and pH_{zpc}) can be found in Supporting Information (Figures S 1 and S 2, Tables S 1 and S 2). The electron crystallography was calculated for four circle diameters and compared to the AMS database.

The coated magnetite nanoparticles (nFe_3O_4@DMSA) were prepared using a ligand exchange reaction of oleic acid for dimercapto-succinic acid (DMSA) following a reported procedure[29,30]. The particle surface was modified with DMSA to offer free ligand groups for biomolecule conjugation and a negative charge at pH 7 that provides a greater stability in aqueous media[30]. Particles were coagulated from the hydrophobic suspension (50 mg/5 mL) by ethanol addition, centrifugation (2825×g, 10 min) and elimination of the solution. A mixture of 25 mL toluene and a solution of 90 mg DMSA in 5 mL dimethylsulfoxide (DMSO) were added to the coagulated particles, which were sonicated (5 min) and stirred mechanically (24 h). Solvent was then discarded, precipitated particles washed and centrifuged three times with an ethanol:acetone mixture (50:50 v/v). nFe_3O_4 coated with DMSA were separated by centrifugation (4000 rpm, 15 min) and washed in Milli-Q water until the washing solutions conductivity were negligible and DOC concentrations below 0.5 ppm. Finally, nanoparticles were dispersed in alkaline water H_2O before dispersion at pH 7. The size distributions for both coated and uncoated nFe_3O_4 were estimated at 11 ± 3 nm and 9 ± 2 nm, respectively, using TEM and Image J (see Figure S 1).

Column Preparations

A total of 9 columns (i.e. 3 experiments in triplicates) was performed in poly(methyl methacrylate)) (PMMA) pipes with an inner diameter of 4 cm and length of 50 cm. The bottom of each of these columns was trimmed to a wedge to facilitate insertion of PTFE cap. Each cap was equipped of polyethylene filter with a porosity of 100 µm (2F Technologies, France).

Natural wetland organic–rich soil from *Pleine-Fougères* (western France, Figure S 3) belonging to the '*Zone Atelier Armorique*' experimental watershed was used as the porous media for all column experiments. The soil sample (i.e. organo-mineral horizon A) was prepared according to the Environmental Protection Agency (EPA) soil sampling protocol (i.e. method 5035)[31]. The soil was dried at 40°C for 72 h and the agglomerates were broken by hand. Particles larger than 2 mm were removed by sieving. The experiments described here were conducted using the soil fraction smaller than 2 mm size. The soil organic matter (SOM) content and granulometric composition were determined at the Central Analysis Laboratory of the *Institut National de la Recherche*

Agronomique (INRA) in Arras (France) (Table S 3). The organic carbon content (Table S 3) and chemical composition (Table S 4) was determined at the '*Service d'Analyse des Roches et des Minéraux*' (SARM) laboratory in Nancy (France), using an oxygen combustion method with a CS analyser (LECO SC 144DRPC).

The packing procedure follows the Organisation for Economic Co-operation and Development (OECD)[32] protocol guideline 312. The columns were packed with sieved soil (<2 mm) up to a height of approximately 38 cm. To obtain uniform packing, the soil was added to the columns in small portions with a spoon and pressed with a plunger under simultaneous gentle column vibration until the top of the soil column does not further sink.

After packing, the soil columns were pre-wetted with artificial rainwater ($5 \bullet 10^{-3}$ M NaCl) from bottom to top to displace the air in the soil pores by water. Thereafter, the soil columns could equilibrate, and the volumes used to wet the soil column (corresponding to 1 pore volume – PV) were measured by weighing the difference after wetting with ultrapure water with an ionic strength settled at $5 \bullet 10^{-3}$ M in NaCl.

Leaching Experiments

To produce data comparable to the literature, the OECD protocol was also used during the leaching soil experiments[32]. A peristaltic pump was used to apply artificial rainwater and the nFe_3O_4 suspensions at 5 $mL \bullet min^{-1}$ (i.e. ~0.4 $mL \bullet min^{-1} \bullet cm^{-2}$). The flow rates were constantly controlled. Three types of experiments were performed with different leaching solutions: (1) a control experiment with synthetic rain water composed of Milli-Q water with an ionic strength (IS) at $5 \bullet 10^{-3}$ M NaCl and a pH at ~ 6.5, (2) an experiment with a suspension of uncoated nFe_3O_4 (IS = $5 \bullet 10^{-3}$ M NaCl, pH ~ 6.5 and [Fe] ~ 20 $mg \bullet L^{-1}$), and (3) an experiment with a suspension of nFe_3O_4@DMSA (IS = $5 \bullet 10^{-3}$M NaCl, pH ~ 6.5 and [Fe] ~ 20 $mg \bullet L^{-1}$). Prior each column experiments (i.e. on the same day), nFe_3O_4 were transferred from gloves box (i.e. nitrogen atmosphere) to a pure water solution (i.e. oxygen atmosphere). The solutions were constantly stirred throughout the leaching experiments. The leaching experiments were performed for 28 h. Only 2 L of water were spiked with both nFe_3O_4. After the two first litters, synthetic water was used (IS = $5 \bullet 10^{-3}$M NaCl, pH ~ 6.5) for the rest of the leaching. The leaching water samples were collected by an Eldex universal fraction collector with an interval time of 10 min per fraction. The initial composition of the leaching solutions for the three exposures are displayed in Table S 5.

Size Fractionation

To evaluate the distribution of TEs and various colloidal pools, the leaching samples were fractionated by size using two cut-offs of 0.22 µm (i.e. <220 nm) and 2 kDa (i.e. <1.6 nm), according to the colloidal phase from 220 nm to 1.6 nm and the 'truly' dissolved fraction below 1.6 nm. The conversion of the molecular weight in nanometre was calculated according Erickson[33]:

$$R_{min} = 0.066\, M^{\frac{1}{3}}$$

Where M is the molecular weight in Dalton and R_{min} is the minimal radius in nanometre. All collected leached water samples were filtrated (i.e. cut-off of 220 nm, polyether sulfone membrane, Sartorius Minisart). Sampling was settled on the leached volume (pore volume, PV). Twelve samples (S1 to S12) were collected for the 220 nm-fraction (PV ≈ 2, 4, 6, 8, 10, 12, 14, 16, 20, 24, 28, 30). Five samples (i.e. PV ≈ 2, 4, 8, 16 and 30; corresponding to S1, S2, S4, S8 and S12;) were fractionated at 1.6 nm by ultrafiltration cells (15 mL centrifugal tubes, Vivaspin). All analyses were performed on these different fractions (i.e. C_{org}, total major and trace element concentrations, aromaticity).

Chemical parameters

Redox (Eh) and pH potential were constantly monitored throughout the experiments. The electrodes were calibrated for each experiment with a WTW (Xylem Analytics, Germany) solution for pH (i.e. 4.01 and 7 at 25 °C) and a potential redox buffer standard (i.e. 220 mV).

Micro-XRF analyses

The soil columns were analysed by micro-X-ray fluorescence spectroscopy at CEREGE (Aix-en-Provence, France). The solid soil sample preparation was adapted from Solovitch et al[11]. Columns containing retained nFe_3O_4 after the experiments were frozen and cut in vertical sections of 9.5 cm by 2 cm thickness. Laboratory-based micro-X-ray fluorescence (µ-XRF) measurements were done on the samples that were kept frozen using a Pelletier cooled sample holder. Measurements were carried out on a HORIBA XGT - 7000 microscope equipped with an X-ray guide tube producing a finely focused and high-intensity beam with a 100 µm spot size and a tension of 50 kV. Each 256 x 266 pixels represents 100 µm. Up to 12 scans were produced for each individual sample with a counting time per frame of 2000 s. Spectral data processing was performed with the software Image J.

Dissolved Organic Carbon (DOC) and Aromaticity

DOC was measured with a Total Organic Carbon analyzer (Shimadzu TOC-5050A). The error on the measurements was below 5% and checked for each analysis. SUVA and aromaticity index were determined by UV absorption analyses performed at 254 nm with a Perkin-Elmer spectrophotometer (More details in ESI - Analysis 1).

Pyrolysis - Gas Chromatography - Mass Spectrometry (Py-GC-MS)

Five PVs were selected to assess the molecular composition of NOM during the leaching experiments (S1, S2, S4, S8, and S12). The samples were fractionated using the large Jumbosep® ultrafiltration system (Pall® Life Sciences), a centrifugal device with the smallest cut-off size available for 60-mL samples (3 kDa = 1.8 nm). To meet the mass required for Py-GC-MS analyses (i.e. ~1 mg dw), sample volumes between 100 and 250 mL, according to the DOC concentration, were filtrated. The samples were then frozen at -20°C and lyophilized (More details in ESI - Analysis 2).

Major and trace elements analyses

Total concentrations of major and trace elements for each PV, fraction and cut-off sizes (i.e. <1.6 nm and between 220 and 1.6 nm) were measured on an ICP-MS (Agilent 7700X). Both filtered

samples were directly acidified with nitric acid (HNO_3; 14.6 N) at 2% v/v prior to ICP-MS analysis. Calibration curves and accuracy controls were performed following Yéghicheyan et al.[34] and using river water reference material for TEs with a large compositional range (SLRS5, National Research Council of Canada). The total relative uncertainties were around 5%.

Results and discussion

Hydrogen (pH) and Redox (Eh) potential

The pH of the leaching water with nFe_3O_4 fluctuated between 5.5 and 6.5 (Figure 1a) and should have consequently contributed to the aggregation of the nFe_3O_4 on the soil surface. Although the pH drives the surface charge of uncoated particles such as nFe_3O_4, negative (i.e. FeO^-) and positive (i.e. $FeOH_2^+$) charges should coexist at the surface of the particles. For instance, the pH of the point of zero charge (pH_{zpc}) of the uncoated nFe_3O_4 was calculated to be $(|pH_1+pH_2|)/2 = pH_{ZPC}$ = 5.1 ± 0.1 according the model 1 site/2 pK model[35] (see Figure S1), which is slightly lower than the values reported in the literature for Fe_3O_4: 5.56[36], 6[37], 7.1[38] and 7.0[39]. However, considering the 1 site/ 1 pK model[35], the pH_{zpc} of our uncoated nFe_3O_4 would be $|pK| = pH_{zpc}$ = 6.70 ± 0.2, which is more consistent with the literature. Therefore, this last value will be used in the present study. According to a measured pH_{zpc} of 6.7 ± 0.2, at pH < pH_{zpc}, the $FeOH_2^+$ groups should dominate the FeO^- groups (i.e., net surface charge is positive). At pH_{zpc}, the number of $FeOH_2^+$ groups should however equal the FeO^- groups. Above pH_{zpc}, FeO^- groups should dominate (i.e. net surface charge is negative). While the net surface charge of nFe_3O_4 is pH-dependent, the soil solid phase charges are more stable, and as such, aggregation between the positively charged magnetite particles and the negatively charged soil particles should take place at pH below the pH_{zpc} of nFe_3O_4[40].

The pH of the leaching solution with nFe_3O_4@DMSA varied between 5.0 and 6.5, which should correspond to a more stable condition for the particles. nFe_3O_4@DMSA have indeed been shown to be stable for months at any pH between 3 and 11[30], with negative charges in the range of pH = 1 - 14 (at pH = 5, Z-potential ~ -35 ± 10 mV)[41]. Although the interactions of nFe_3O_4@DMSA with other particles are also strongly dependent on the pH, their coating should nevertheless enhanced their stability due to steric hindrance or combined electrostatic and steric (electrosteric) effects[40]. As such, nFe_3O_4@DMSA are expected to be more dispersed for a wider range of pH. DMSA monomers are small molecules that have the capacity to complex with iron oxides via their thiol groups (pKa_{SH}= 9.65 et 12.05), which slightly disturbs the structure of the nano-FeO surface and allows a good dispersion of the suspension through the -COO^- functions (pka_{COOH} = 2.71; 3.43)[42].

The pH of the leaching solution during the control experiment varied between 4.7 and 5.1, which is ~1 pH unit below the pH of the leaching solution during experiments with both nFe_3O_4 (i.e. between 5.5 to 6.5 and 5.0 to 6.5 for coated and uncoated, respectively). The higher pH values observed in presence of

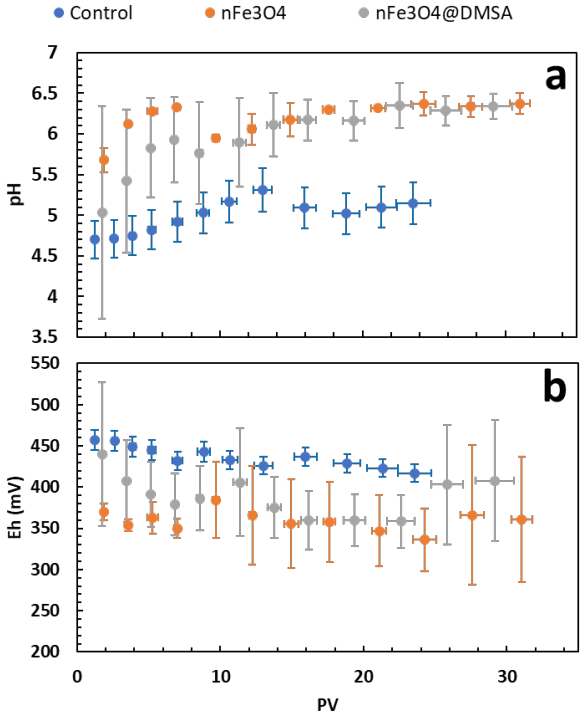

Figure 1. a) pH and b) Eh recorded during the leaching experiment at the output of the columns.

both nFe_3O_4 after 10 PVs (t-test, p-values<0.05) might be the consequence of an oxidation of the nFe_3O_4. Peng et al. [43,44] demonstrated that at pH 6, proton-promoted dissolution yields the release of $Fe^{2+}_{(aq)}$ from magnetite nanoparticles, following the equation 1:

$$Fe^{3+}Fe^{3+}Fe^{2+} + 2H^+ \rightarrow \frac{3}{4}Fe^{3+}Fe^{3+}_{5/3}Fe^{3+}_{1/3}\square_{1/3}O_4^{2-} + H_2O + Fe^{2+} \quad (1)$$

where the square represents a cationic vacancy due to diffusive migration of iron cations[43,44]. Although the pH values observed during the leaching with both particles are similar, in the 10 first PVs the pH values of the leaching solution observed in presence of nFe_3O_4@DMSA were lower. This might be due to the DMSA coating potentially slowing down the proton-promoted dissolution reaction at the beginning of the leaching.

Eh values measured during the leaching experiements were between 350 and 457 mV and were relatively constant throughout the experiments. The values observed during the leaching with both coated and uncoated nFe_3O_4 were between 350 and 440 mV for both coated and uncoated nFe_3O_4 leaching with, and between 417 and 457 mV mV during the control leaching experiment. Although it is difficult to accuratly assess in the soil matrix, such pH and Eh values (pH = 4.6 – 6.5; Eh > 0.3 V) should favour the speciation of iron towards the form Fe^{3+}. In summary, while nFe_3O_4@DMSA particles are expected to be relatively stable, aggregation of uncoated nFe_3O_4 is expected to occur. The redox potential should also push the speciation of iron to be ionic and potentially release iron from nFe_3O_4 particles directly in the leaching solution.

Fe behaviour and mobility.

Total iron (Fe_t, < 220 nm) leached during the experiments showed distinctive patterns (Figure 2a) with total masses of 5.4 ± 0.3, 9.6 ± 3.4 and 21 ± 7.8 mg for the control, uncoated nF_3O_4, and nFe_3O_4@DMSA, respectively (Table S 6). The controls showed a relatively constant release of Fe_t leached during the experiments, while leaching with uncoated nFe_3O_4 and with nFe_3O_4@DMSA showed massive released of Fe_t in the 10 first PVs. Previous studies that have performed such experiments, but using standardized artificial sand columns, described such patterns using the Attachment Efficiency (AE), which has been suggested as an appropriate fate descriptor for transport of engineered nanoparticles (ENPs) in soils[45,46]. The different results for the different nanoparticles that are presented here, highlight however that the complexity of natural soils makes difficult the description of such patterns using a single parameter and that AE should be defined for unique combination of ENP and soil. As such, the transport predictions of ENPs using AE appears unreliable, due to the important number of parameters influencing AE such as the ionic strength, natural organic matter (NOM), soil composition and temperature[46].

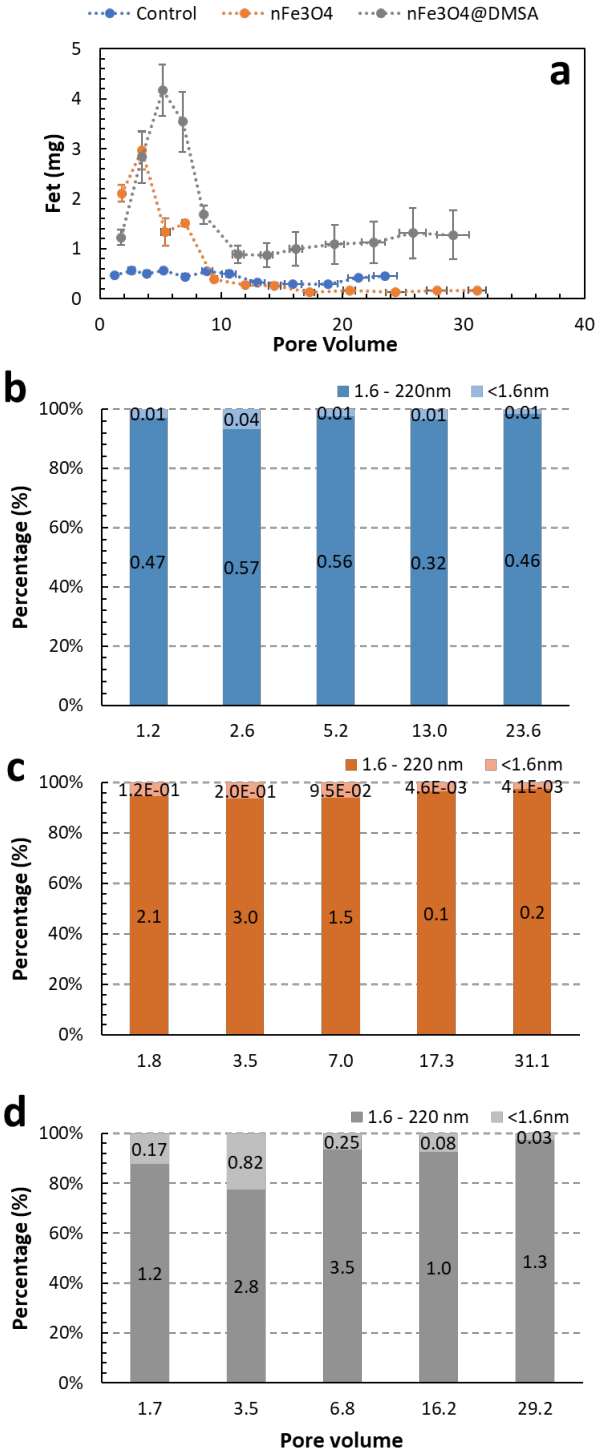

Figure 2. a) Total iron leached < 220 nm with in blue the control, orange bare nFe_3O_4 and grey nFe_3O_4@DMSA; b) Size distribution of Fe for the control within the leaching; c). Size distribution of Fe for the nFe_3O_4 within the leaching; d) Size distribution of Fe for nFe_3O_4@DMSA within the leaching; The labelled in the histograms are the Fe mass in mg in each fraction.

In the columns with uncoated nFe_3O_4 and nFe_3O_4@DMSA, respectively, about 87 to 98 % and 71 to 97 % of the leached Fe_t were leached within the 220 nm to 1.6 nm fraction, suggesting a strong movement of nanoparticles or of natural colloids (Figure 2 b, c, d). The size of the Fe_t leached during the experiments was relatively constant for the columns with uncoated nFe_3O_4 with a proportion of 87 to 98 % between 1.6 and 220 nm (Figure 2c). The size of the leached Fe_t in the columns with nFe_3O_4@DMSA showed however more difference. A larger proportion of Fe_t leached in the 10 first PV was below 1.6 nm (between 14 and 29 %, Figure 2d). These distinct patterns might be explained by different retention times for nFe_3O_4 and nFe_3O_4@DMSA on the columns. We suggest that the Fe_t in the size fraction below 1.6 nm released at the beginning of the leaching with nFe_3O_4@DMSA might be a "dissolved" Fe (i.e Fe^{2+}) released from the oxidation of magnetite to maghemite (as described by equation 1). In presence of nFe_3O_4@DMSA particles, DMSA might be complexed the Fe^{2+}, and leached in the small fraction (< 1.6 nm).

µ-XRF analyses on the first 5 cm of the columns showed very distinct patterns for the controls, the leaching with uncoated nFe_3O_4, and the leaching with nFe_3O_4@DMSA (Figure 3). For instance, the results showed an important peak of Fe in columns with nFe_3O_4 (orange line), while the Fe distribution was more constant for the control leaching (blue line) and the leaching with nFe_3O_4@DMSA (grey line). Hence, nFe_3O_4@DMSA seems to have been transported lower in the column, bellow the first 5 cm, by contrast to uncoated nFe_3O_4, no Fe peak was detected on µ-XRF analyses (grey line). Also, after 1.5 cm the homogenous distribution of Fe of nFe_3O_4@DMSA show similar amount of Fe than for nFe_3O_4. The different patterns could be explained by a better transport of nFe_3O_4@DMSA through the column due to a better stability of the particles improved by the DMSA coating[47,48].

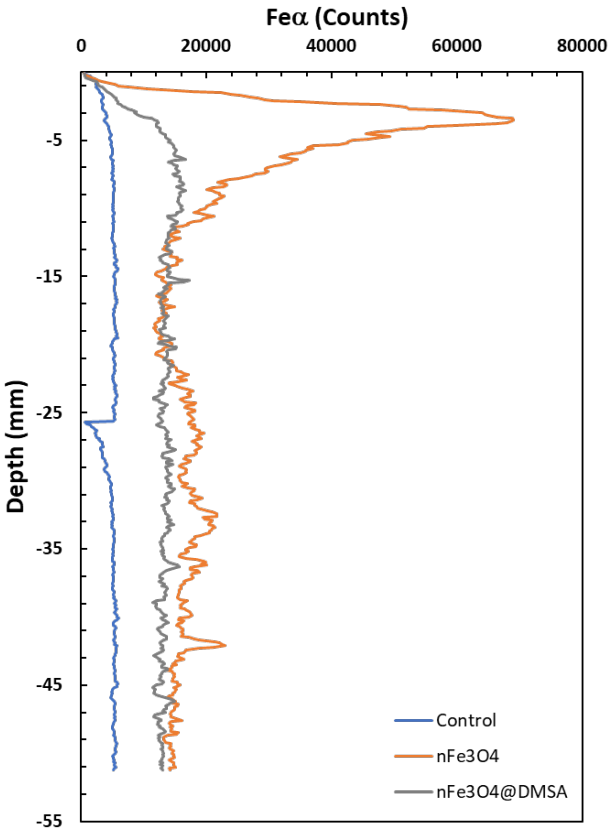

Figure 3. Distribution of iron (Fe) in the soil column (solid phase) by µXRF analysis. in Bleu: Control leaching; Orange: uncoated nFe_3O_4 leaching and Grey: DMSA-coated nFe_3O_4 leaching

Organic carbon

DOC measurements have shown distinct total dissolved organic carbon (DOC_t, i.e. <220nm, Figure 4) patterns in the different leaching experiments. For instance, the amount of DOC_t leached in presence of nFe_3O_4@DMSA was much higher than in presence of uncoated nFe_3O_4 or during the control experiment. Specifically, $0.99 \pm 4.9 \times 10^{-2}$, $0.54 \pm 8.5 \times 10^{-2}$, and $1.7 \pm 2.2 \times 10^{-2}$ g of DOC was leached during the control, nFe_3O_4 and nFe_3O_4@DMSA leaching experiments, respectively (Table S 6). This suggests an enhanced sequestration of the DOC_t in presence of the uncoated nFe_3O_4, whereas the presence of nFe_3O_4@DMSA seems, in the contrary, to highly mobilize the DOC_t (Figure 4a). As both nFe_3O_4@DMSA and DOC_t are negatively charged, this might be explained by a competition on soil particle sites (positively charged). However, we suggest that a part of this signal is probably also due to the organic coating from the particles itself.

The aromaticity of DOC_t during the control experiments increased to reach a stable aromaticity level of about 25 % after 15 PV (Figure 4b). A large proportion (from 60 to 78 %) of the molecules were below 1.6 nm. The aromaticity of DOC_t during the leaching experiments with uncoated nFe_3O_4 was similar to the control experiments, reaching quickly an aromaticity between 20 and 30 % after 3 PV and stayed relatively constant until the end of the leaching (Figure 4b). 53 to 73 % of molecules were below 1.6 nm. By contrast, the leaching experiments with nFe_3O_4@DMSA show a distinct pattern with a very low aromaticity in the 10 first PV (i.e. below 15 %) reaching about 25 % after the first 12 PV (Figure 4b). Between 60 to 95 % of the molecules were below 1.6 nm. The low aromaticity observed in the leaching experiments with nFe_3O_4@DMSA might be simply due to a destabilization of the DMSA coating driving the aromaticity down. This is supported by Py-GCMS analyses done on fraction below 1.8 nm, in which DMSA was detected in the 10 first PVs (Figure S 4).

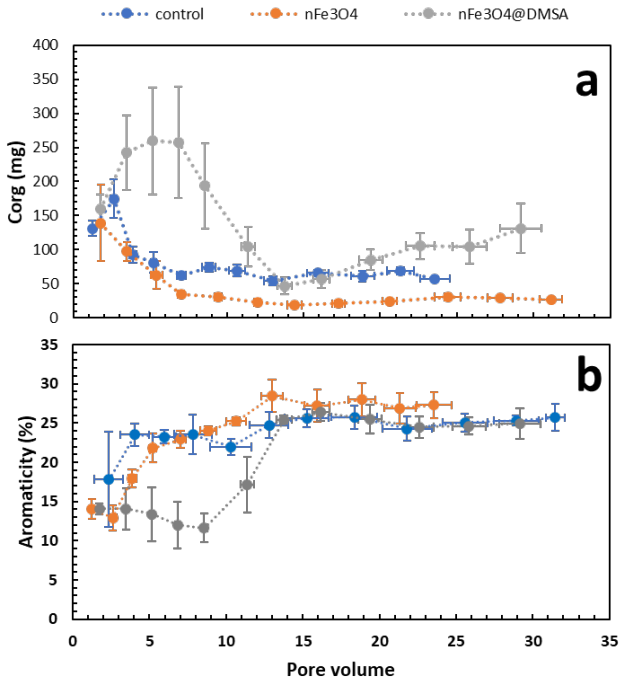

Figure 4. Leaching of (a) amount of organic carbon (C_{org}) < 220nm and respectively (b) the aromaticity of the C_{org} during each leaching.

The specific molecular composition of the size fraction below 1.8 nm also suggests that both nFe_3O_4 had an impact on the movement of the DOC < 1.8 nm during the leaching experiments. The molecular composition of the control leaching was mostly composed of lignin and carbohydrates in the first part of the leaching and the proportion of fatty acids increased with PVs (Figure S 4). Although carbohydrates and lignin still represent a major part of the DOC_t < 1.8 nmleached in presence of uncoated nFe_3O_4, the proportions of molecular groups are strongly affected. For instance, the contribution of fatty acids (e.g. PV = 17.3 and 31.1, 69 and 36 %, respectively) and small acids (e.g. PV = 7, 33 %) increased importantly (Figure S 4). This support the idea that the surface charge of the uncoated nFe_3O_4 might compete with other molecules (e.g. carbohydrates and acids) for bonding with the soil particles. In fact, fractionation by molecular weight (MW) may be induced by the sorption of NOM onto iron oxides[49]. It seems that high MW fractions (m/z ≈ 1700 Da) are more prone to sorption, while intermediate MW

fractions (IMW; m/z ≈ 900 Da) are more hydrophilic[50,51]. Such competition should indeed contribute to the leaching of molecules normally bounded to the soil particles. An important amount of DMSA was also detected during the first part (i.e. PV ≈ 1.7, 3.5, and 6.7 of the leaching experiments in presence of coated nFe_3O_4, suggesting a desorption of the DMSA coating.

TEs dynamics

The analysis of the elemental concentrations during the control leaching experiment (Figure 5, blue bars) showed that all elements in the size fraction between 1.6 and 220 nm were not correlated with the concentration of Fe, while some elements including Cd, Mg, Si, Ca, Sr, Ba and U were correlated with the amount of DOC_t (p-values < 0.05, t-test). The introduction of uncoated nFe_3O_4 (Figure 5, orange bars) in the columns changed the behaviour of the elements. A strong correlation between all element (excepted Ca) and Fe concentrations is indeed suggested (p-values < 0.05, t-test). Still in presence of nFe_3O_4, heavy metals, trivalent, oxyanions (excepted B and Sb) and others (Be, Si) are correlated with the DOC_t (p-values < 0.05, t-test). We suggest that nFe_3O_4 scavenge elements and DOC during the oxidation process of magnetite into maghemite, transporting them into the leaching solution. The introduction of nFe_3O_4@DMSA (Figure 5, grey bars) in the columns suggests more selective effects. Elements such as Mn, Mg, Ca, Sr and Ba are anti-correlated with Fe (p-values < 0.05, t-test). Anti-correlation with DOC_t is also observed with Li and As (p-values < 0.05). The data suggests that other oxyanions, heavy metals and elements are only weakly anticorrelated with the DOC_t.

A clear perturbation of TEs behaviour is observed when both types of nFe_3O_4 are introduced in the system. However, the elemental interactions are clearly different and driven by the surface compositions of the particles. The introduction of uncoated nFe_3O_4 shows high interactions with almost all elements and might be attributed to a potential adsorption of those elements on the uncoated particles and consequently leading to a sequestration of those elements. The introduction of coated nFe_3O_4 shows more selective interactions but may still have promoted their mobility in the soil matrix.

TEs sequestration

The amount of TEs leached and monitored throughout the experiments evidenced that the surface composition of nFe_3O_4 influences the fate (Figure 6) and the behaviour (Figure S 5) of TEs in soil. The presence of both uncoated nFe_3O_4 (orange bars) and nFe_3O_4@DMSA (grey bars) led to less TEs leached as compared to the control experiment (blue bars, Figure 6). Although the amount of TEs leached in presence of both

nFe_3O_4 revealed a comparable level sequestration, the presence of uncoated nFe_3O_4 seems to have induced the sequestration of more TEs than the presence of coated particles, notably for some TEs such as Ba, Li, Rb, Sr, Zn, Sc, Be (Figures 6a, b), trivalent such as Al, REEs, Y (Figures 7c, d), oxyanions As, V, Sb (Figures 6 e, f), heavy metals Co, Cu, Ni, Pb (Figure 6 g) and finally U (Figure 6h). Examples of TEs behaviours

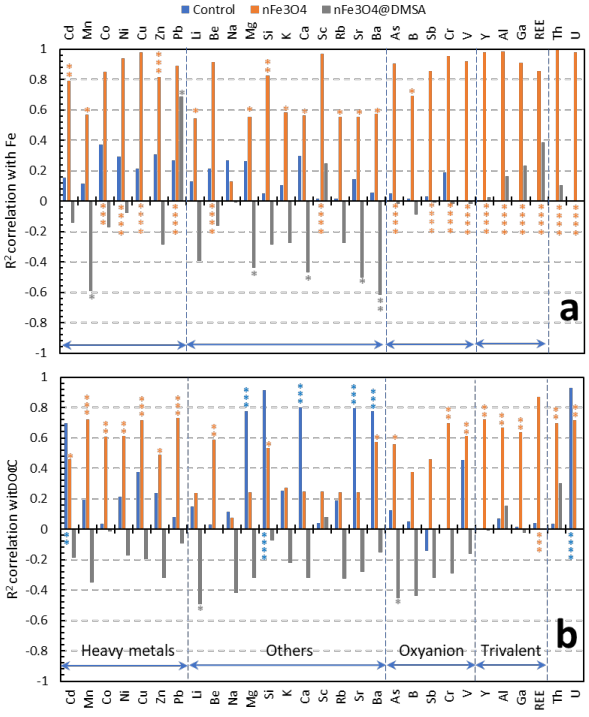

Figure 5. square R correlation of trace element concentrations below 0.22nm with (a) iron concentration, (b) dissolved organic carbon. Blue bars are control leaching, grey nFe_3O_4@DMSA leaching and orange are pristine nFe_3O_4 leaching. P-values are like follow: * p<0.05, ** p<0.01, *** p<0.0001, **** p<0.0001.

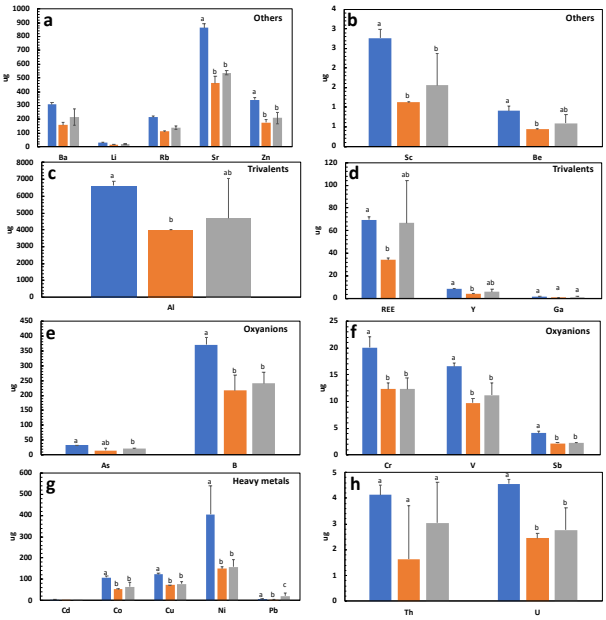

Figure 6. Total amount of TEs leached at the end of the experiments; following Figure 5, a) and b) refers to "others" TEs, c) and d) trivalent elements; e and f) oxyanions, g) heavy metals and h) Th and U. Blue bars represent the control experiment, orange bars the experiment in presence of nFe_3O_4 and grey bars the experiment in presence of nFe_3O_4@DMSA. Numbers with different letters are significantly different (p<0.05).

during the leaching are given in Figure S 5. For instance, heavy metals (e.g. Cu) and oxyanions (e.g. As) have similar patterns with a stronger leaching during the first 5 PVs. Interestingly, REEs have more distinct patterns, where in presence of nFe_3O_4@DMSA their leaching is identical to the release of DOC (Figure 4a). We suggest that this is could be due to the complexation of REEs with DOC as often previously evidenced[52]. Potentially, the leaching of DOC in presence of nFe_3O_4@DMSA may contribute to carry REEs in the colloidal phase.

Conclusions: Environmental implications

Considering that about 40 mg of Fe were applied to the columns in the form of nFe_3O_4 during the leaching experiments, our results suggest that a large part of nFe_3O_4, coated and uncoated, might have been sequestered during the leaching. We suggest that this might be due to an aggregation or sorption mechanisms in contact with soil components as NOM into the soil columns. However, it is likely that such bindings could be broken by longer leaching, change in redox and pH conditions[53]. nFe_3O_4 are known to be excellent TEs adsorbent and because we observed some TEs leached with different behaviour during the experiments, it is essential to further investigate the change in TEs mobility associated with the nanoparticle coating[54].

The leaching experiments within natural soil matrix evidenced that the nFe_3O_4 surface composition - and not only the presence of nFe_3O_4 - has an impact on the TEs mobility and that the surface composition could be involved in a transfer of TEs into deeper soil horizon or groundwater. In general, we observe a weaker solubilisation of the TEs in presence nanoparticles (i.e. nFe_3O_4 < nFe_3O_4@DMSA < control). Importantly, the results also suggest that within a natural soil matrix, nanoparticle surface composition (i.e. coating) can be unstable and potentially having important consequence regarding the TEs mobility interacting with it. Elements such as As, Pb or Fe^{2+} could be complexed with eventually destabilized DMSA coating, known to easily complex with those metals in simple matrix (i.e. sand)[55]. Most of column studies pointed out the strong capacity of iron oxides nanoparticles coated (i.e. humic acid) to remove from the soil water toxic metals such as Hg, Pb, Cd, As, or Cu[55]. However, to our knowledge, all these studies used simple matrix such as sand particles. Here, in a natural matrix soil, we observed that elements such as Pb or Cd are contrarily more extensively mobilized during the leaching in presence of nFe_3O_4. We suggest that these different behaviours might be due to (i) the destabilization of the coating from the coated nFe_3O_4 that might complex with these TEs and leach more easily in the soil and (ii) the release of natural colloids favouring the mobility of some TEs normally interacting with NOM or natural Fe nano-oxides. This highlights that the aging of the nanoparticles is a critical issue concerning the fate of TEs in soil horizons and groundwaters. As such, the life cycle of nanoparticles must be seriously considered regarding the use of iron oxides nanoparticles to remove toxic metals from contaminated soils.

Conflicts of interest

In accordance with our policy on Conflicts of interest please ensure that a conflicts of interest statement is included in your manuscript here. Please note that this statement is required for all submitted manuscripts. If no conflicts exist, please state that "There are no conflicts to declare".

Acknowledgements

We are thankful to Dr Jérôme Labille and Dr Armand Masion (CEREGE) for thorough advices on the sample preparation for µXRF analysis performed with Perrine Chaurand (CEREGE). The authors also thank Dr Jérôme Rose (CEREGE) for his help during the µXRF measurements and the resulting data analysis. The authors are also grateful for his constructive comments and support during the writing of the manuscript. Pascal Rolland and Xavier Le Coz are deeply acknowledged for column designing and soil samples preparation, respectively. Dr Jean-Noël Proust and Jean-Jacques Kermarrec (Géosciences Rennes) are thanked for their kind help in solid sample preparation for further analysis. We are also grateful to Yannick Fauvel from the INRA SAS Research unit (Rennes) for a fraction collector lending. This study was funded by the CNRS-INSU/INEE EC2CO program through 'NanoOrgaTraces' project awarded to Mathieu Pédrot.

References

1 N. Mueller and B. Nowack, *Environ. Sci. Technol.*, 2008, **42**, 44447–53.

2 C. Coll, D. Notter, F. Gottschalk, T. Sun, C. Som and B. Nowack, *Nanotoxicology*, 2015, **5390**, 1–9.

3 Y. Wang, L. Deng, A. Caballero-Guzman and B. Nowack, *Nanotoxicology*, 2016, **10**, 1545–1554.

4 M. R. Wiesner, G. V. Lowry, P. Alvarez, D. Dionysiou and P. Biswas, *Environ. Sci. Technol.*, 2006, **40**, 4336–4345.

5 M. Auffan, J. Rose, J.-Y. Bottero, G. V Lowry, J.-P. Jolivet and M. R. Wiesner, *Nat. Nanotechnol.*, 2009, **4**, 634–41.

6 M. Hua, S. Zhang, B. Pan, W. Zhang, L. Lv and Q. Zhang, *J. Hazard. Mater.*, 2012, **211**–**212**, 317–31.

7 M. Auffan, J. Rose, O. Proux, A. Masion, W. Liu, L. Benameur, F. Ziarelli, A. Botta, C. Chaneac and J.-Y. Bottero, *Environ. Sci. Technol.*, 2012, **46**, 10789–10796.

8 M. Auffan, J. Rose, O. Proux, D. Borschneck, A. Masion, P. Chaurand, J.-L. Hazemann, C. Chaneac, J.-P. Jolivet, Mark R. Wiesner, A. Van Geen and J.-Y. Bottero, *Langmuir*, 2008, **24**, 3215–3222.

9 W. Yan, M. A. V. Ramos, B. E. Koel and W. Zhang, *J. Phys. Chem. C*, 2012, **116**, 5303–5311.

10 L. Carlos, F. Einschlag S. García, M. C. González and D. O. Mártire, *Waste Water - Treatment Technologies and Recent Analytical Developments*, InTech, 2013.

11 N. Solovitch, J. Labille, J. Rose, P. Chaurand, D. Borschneck,

M. R. Wiesner and J.-Y. Bottero, *Environ. Sci. Technol.*, 2010, **44**, 4897–4902.

12 K. A. D. Guzman, M. P. Finnegan and J. F. Banfield, *Environ. Sci. Technol.*, 2006, **40**, 7688–7693.

13 S. R. Kanel, D. Nepal, B. Manning and H. Choi, *J. Nanoparticle Res.*, 2007, **9**, 725–735.

14 J. Shang, C. Liu, Z. Wang, H. Wu, K. Zhu, J. Li and J. Liu, .

15 C. Shani, N. Weisbrod and A. Yakirevich, *Colloids Surfaces A Physicochem. Eng. Asp.*, 2008, **316**, 142–150.

16 B. Uyusur, C. J. G. Darnault, P. T. Snee, E. Kokën, A. R. Jacobson and R. R. Wells, *J. Contam. Hydrol.*, 2010, **118**, 184–198.

17 O. Sagee, I. Dror and B. Berkowitz, *Chemosphere*, 2012, **88**, 670–675.

18 M. A. Al-Wabel, D. M. Heil, D. G. Westfall and K. A. Barbarick, *J. Environ. Qual.*, 2002, **31**, 1157–1165.

19 P. Langner, C. Mikutta and R. Kretzschmar, *Nat. Geosci.*, 2011, **5**, 66–73.

20 P. Langner, C. Mikutta and R. Kretzschmar, *Environ. Sci. Technol.*, 2014, **48**, 2281–2289.

21 R. Dahlqvist, K. Andersson, J. Ingri, T. Larsson, B. Stolpe and D. Turner, *Geochim. Cosmochim. Acta*, 2007, **71**, 5339–5354.

22 M. Pédrot, A. Dia, M. Davranche, M. Bouhnik-Le Coz, O. Henin and G. Gruau, *J. Colloid Interface Sci.*, 2008, **325**, 187–197.

23 J. F. McCarthy and J. M. Zachara, *Environ. Sci. Technol.*, 1989, **23**, 496–502.

24 G. Tyler, *Geoderma*, 2004, **119**, 277–290.

25 J. Buffle and R. DeVitre, *Chemical and Biological Regulation of Aquatic Systems*, CRC Press, 1993.

26 V. K. Sharma and M. Sohn, *Environ. Int.*, 2009, **35**, 743–759.

27 R. Massart, *IEEE Trans. Magn.*, 1981, **17**, 1247–1248.

28 E. Duguet, S. Vasseur, S. Mornet, G. Goglio, A. Demourgues, J. Portier, F. Grasset, P. Veverka and E. Pollert, *Bull. Mater. Sci.*, 2006, **29**, 581–586.

29 Y.-W. Jun, Y.-M. Huh, J.-S. Choi, J.-H. Lee, H.-T. Song, S. Kim, S. Yoon, K.-S. Kim, J.-S. Shin, J.-S. Suh and J. Cheon, *J. Am. Chem. Soc.*, 2005, **127**, 5732–5733.

30 A. G. Roca, S. Veintemillas-Verdaguer, M. Port, C. Robic, C. J. Serna and M. P. Morales, *J. Phys. Chem. B*, 2009, **113**, 7033–7039.

31 K. Simmons, J. Deatrick and B. Lewis, *Soil Sampling*, Athens, Gergia, 2014.

32 OECD, in *OECD Guidelines for the Testing of Chemicals*, OECD Publishing, Paris, OECD plubl., 2004.

33 H. P. Erickson, *Biol. Proced. Online*, 2009, **11**, 32–51.

34 D. Yeghicheyan, C. Bossy, M. Bouhnik Le Coz, C. Douchet, G. Granier, A. Heimburger, F. Lacan, A. Lanzanova, T. C. C. Rousseau, J.-L. Seidel, M. Tharaud, F. Candaudap, J. Chmeleff, C. Cloquet, S. Delpoux, M. Labatut, R. Losno, C. Pradoux, Y. Sivry and J. E. Sonke, *Geostand. Geoanalytical Res.*, 2013, **37**, 449–467.

35 K. Bourikas, J. Vakros, C. Kordulis and A. Lycourghiotis, *J. Phys. Chem. B*, 2003, **107**, 9441–9451.

36 M. Chang and Y. hsin Shih, *J. Environ. Manage.*, , DOI:10.1016/j.jenvman.2018.07.021.

37 Z. Lu, Y. Qin, J. Fang, J. Sun, J. Li, F. Liu and W. Yang, *Nanotechnology*, 2008, **19**, 055602.

38 V. Srivastava, P. Singh, C. Weng and Y. Sharma, *Polish J. Chem. Technol.*, , DOI:10.2478/v10026-011-0015-8.

39 L. Agustí, A. Bonaterra, C. Moragrega, J. Camps and E. Montesinos, *J. Plant Pathol.*

40 E. Tombácz, A. Majzik, Z. Horvát and E. Illés, *Rom. Reports Phys.*, 2006, **58**, 281–286.

41 Z. P. Chen, Y. Zhang, S. Zhang, J. G. Xia, J. W. Liu, K. Xu and N. Gu, *Colloids Surfaces A Physicochem. Eng. Asp.*, 2008, **316**, 210–216.

42 M. Auffan, L. Decome, J. Rose, T. Orsiere, M. De Meo, V. Briois, C. Chaneac, L. Olivi, J. Berge-lefranc, A. Botta, M. R. Wiesner and J. Bottero, *Environ. Sci. Technol.*, 2006, **40**, 4367–4373.

43 H. Peng, C. I. Pearce, A. T. N'Diaye, J. Ni, Z. Zhu, J. Liu and K. M. Rosso, *Environ. Sci. Technol.*, , DOI:10.1021/acs.est.8b05098.

44 H. Peng, C. I. Pearce, W. Huang, Z. Zhu, A. T. N'Diaye, K. M. Rosso and J. Liu, *Environ. Sci. Nano*, 2018, **5**, 1545–1555.

45 S. Treumann, S. Torkzaban, S. A. Bradford, R. M. Visalakshan and D. Page, *J. Contam. Hydrol.*, 2014, **164**, 219—229.

46 W. Zhang, J. Crittenden, K. Li and Y. Chen, *Environ. Sci. Technol.*, 2012, **46**, 7054–7062.

47 R. L. Johnson, G. O. Johnson, J. T. Nurmi and P. G. Tratnyek, *Environ. Sci. Technol.*, 2009, **43**, 5455–5460.

48 W. Yantasee, C. L. Warner, T. Sangvanich, R. S. Addleman, T. G. Carter, R. J. Wiacek, G. E. Fryxell, C. Timchalk and M. G. Warner, *Environ. Sci. Technol.*, 2007, **41**, 5114–5119.

49 J. Hur and M. A. Schlautman, *J. Colloid Interface Sci.*, 2003, **264**, 313–321.

50 P. Reiller, B. Amekraz and C. Moulin, *Environ. Sci. Technol.*, 2006, **40**, 2235–2241.

51 F. Claret, T. Schäfer, J. Brevet and P. E. Reiller, *Environ. Sci. Technol.*, 2008, **42**, 8809–8815.

52 O. Pourret, M. Davranche, G. Gruau and A. Dia, *Chem. Geol.*, 2007, **243**, 128–141.

53 M. Baalousha, *Sci. Total Environ.*, 2009, **407**, 2093–2101.

54 R. P. Zito and H. J. Shipley, *RSC Adv.*, 2015, **5**, 29885–29907.

55 J. Liu, Z. Zhao and G. Jiang, *Environ. Sci. Technol.*, 2008, **42**, 6949–6954.

Supporting information

Trace element mobility impacted by Fe_3O_4-nanoparticles surface coating within wetland soil

Maya Al-Sid-Cheikh[a,§], Mathieu Pédrot[a], Aline Dia[a], Mélanie Davranche[a], Laurent Jeanneau[a], Patrice Petitjean[a], Martine Bouhnik-Le Coz[a], Marc-André Cormier[b,c] and Fabien Grasset[d,e]*

Contents

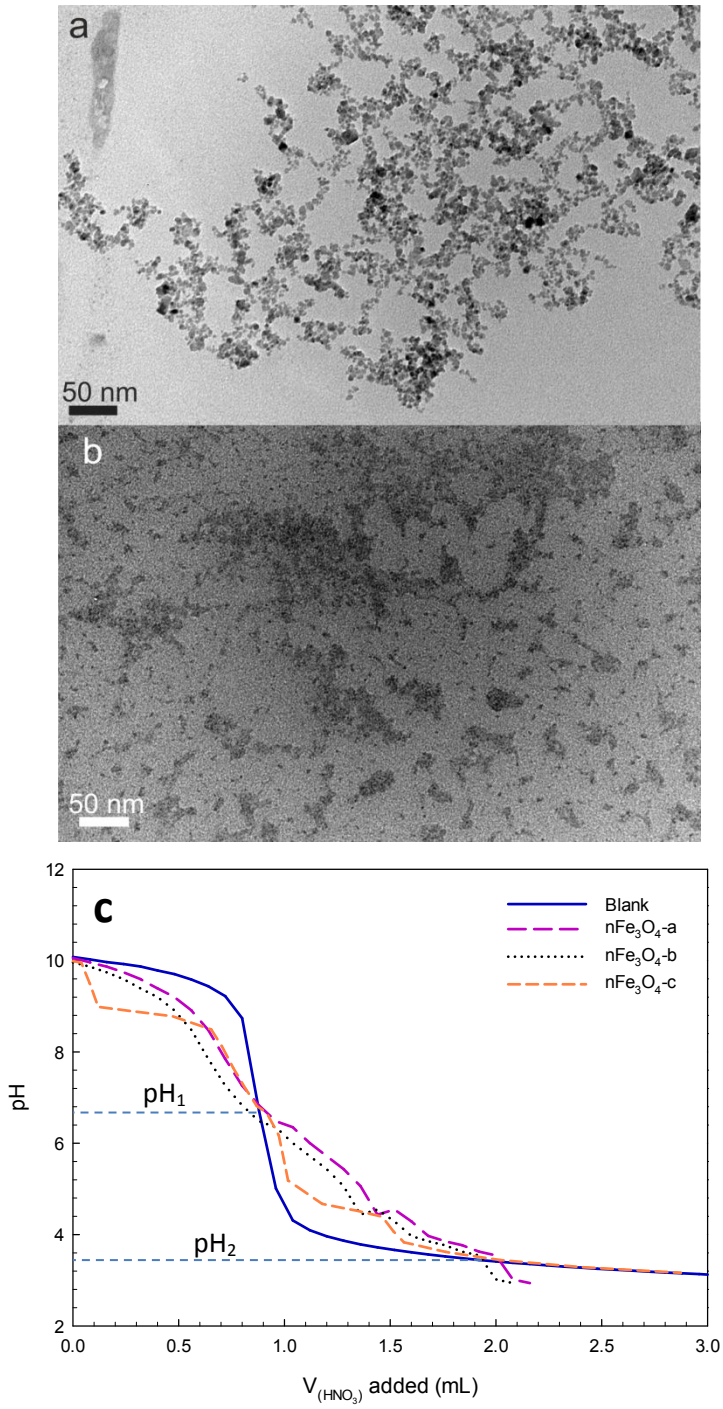

Figure S 1. TEM images of uncoated and DMSA coated nano-Fe_3O_4 (a) uncoated and (b) coated, respectively. C) Characterization of pH_{zpc} of uncoated nFe_3O_4 according to Bourikas, et al. (2003), called differential potentiometric titration (DPT) for uncoated nano-Fe_3O_4. Three replicates were performed called nano-Fe_3O_4_a, nano-Fe_3O_4_b and nano-Fe_3O_4_c.

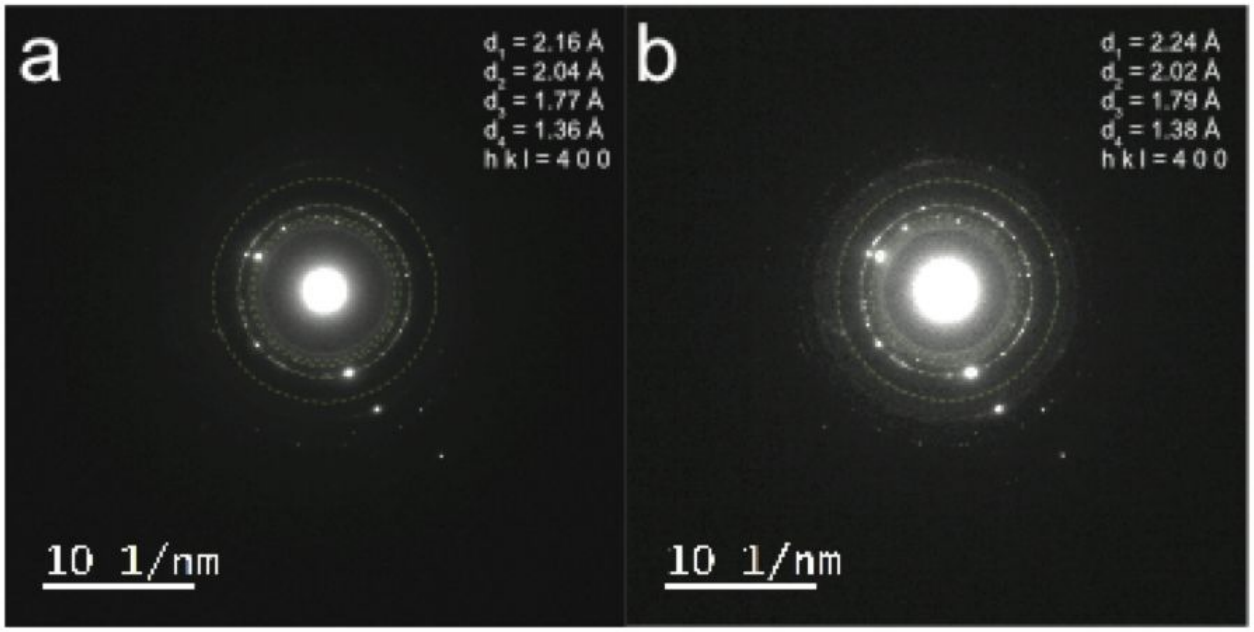

Figure S 2. XRD images from a) uncoated nFe_3O_4 and b) coated nFe_3O_4 with d-spacing calculated for the four first circles (i.e. green dot) and the comparison with AMS database gives magnetite crystallography structure, with h k l: 4 0 0.

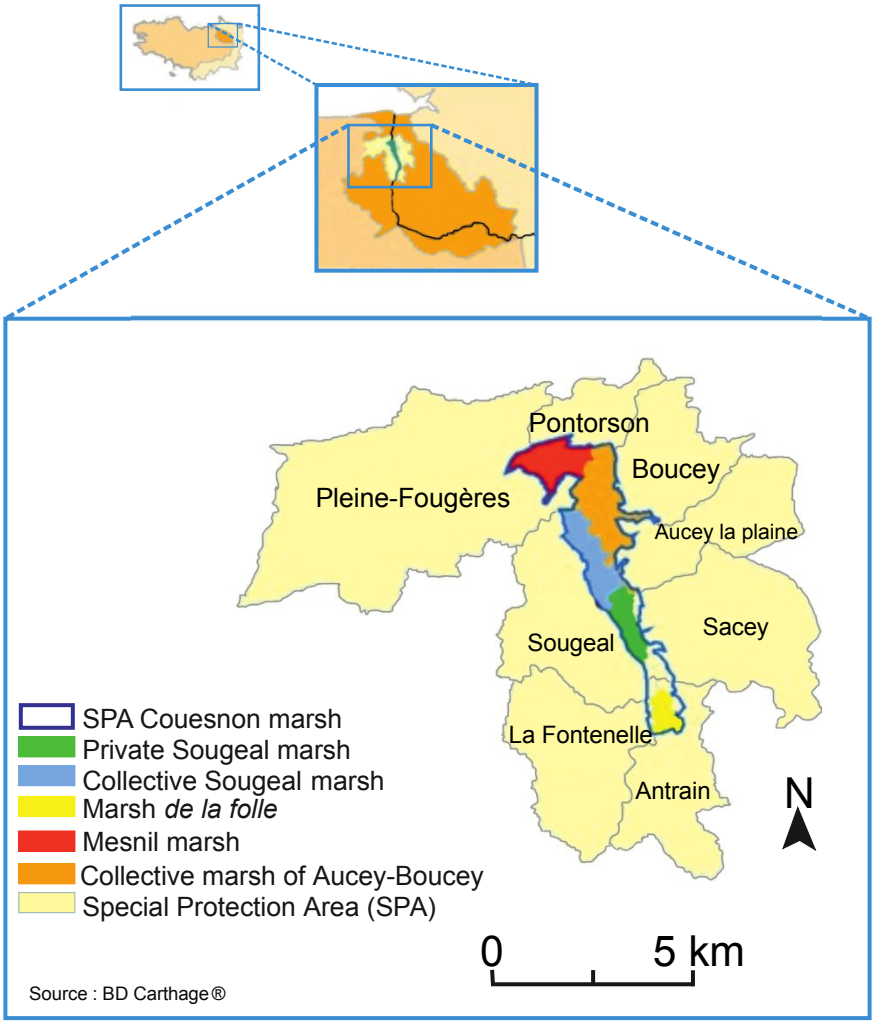

Figure S 3. Study site of the experimental watershed of Pleine-Fougères, Western France.

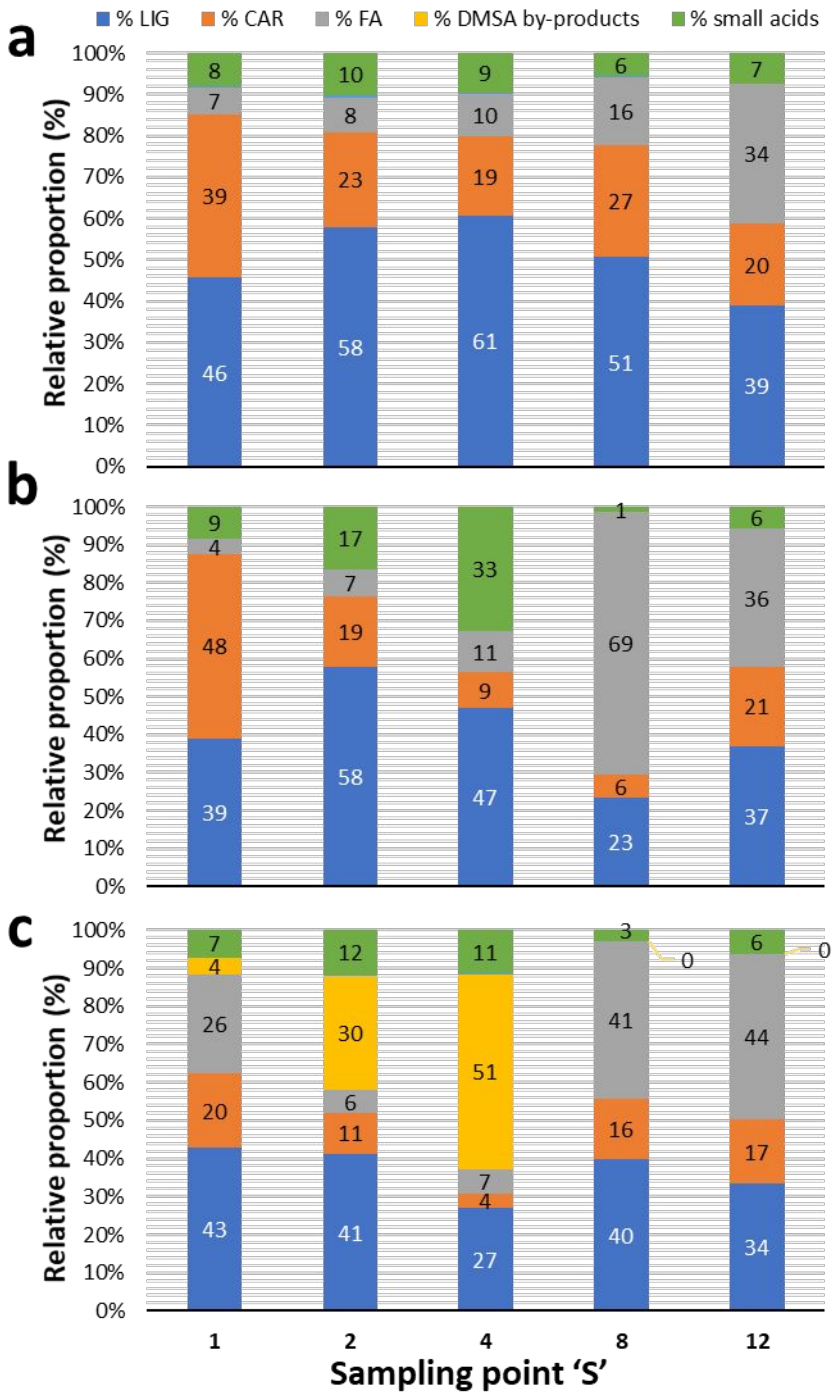

Figure S 4. Py-GCMS analyses for a) Control; b) nFe_3O_4 uncoated and c) nFe_3O_4@DMSA. The labels are the percentage for each compound.

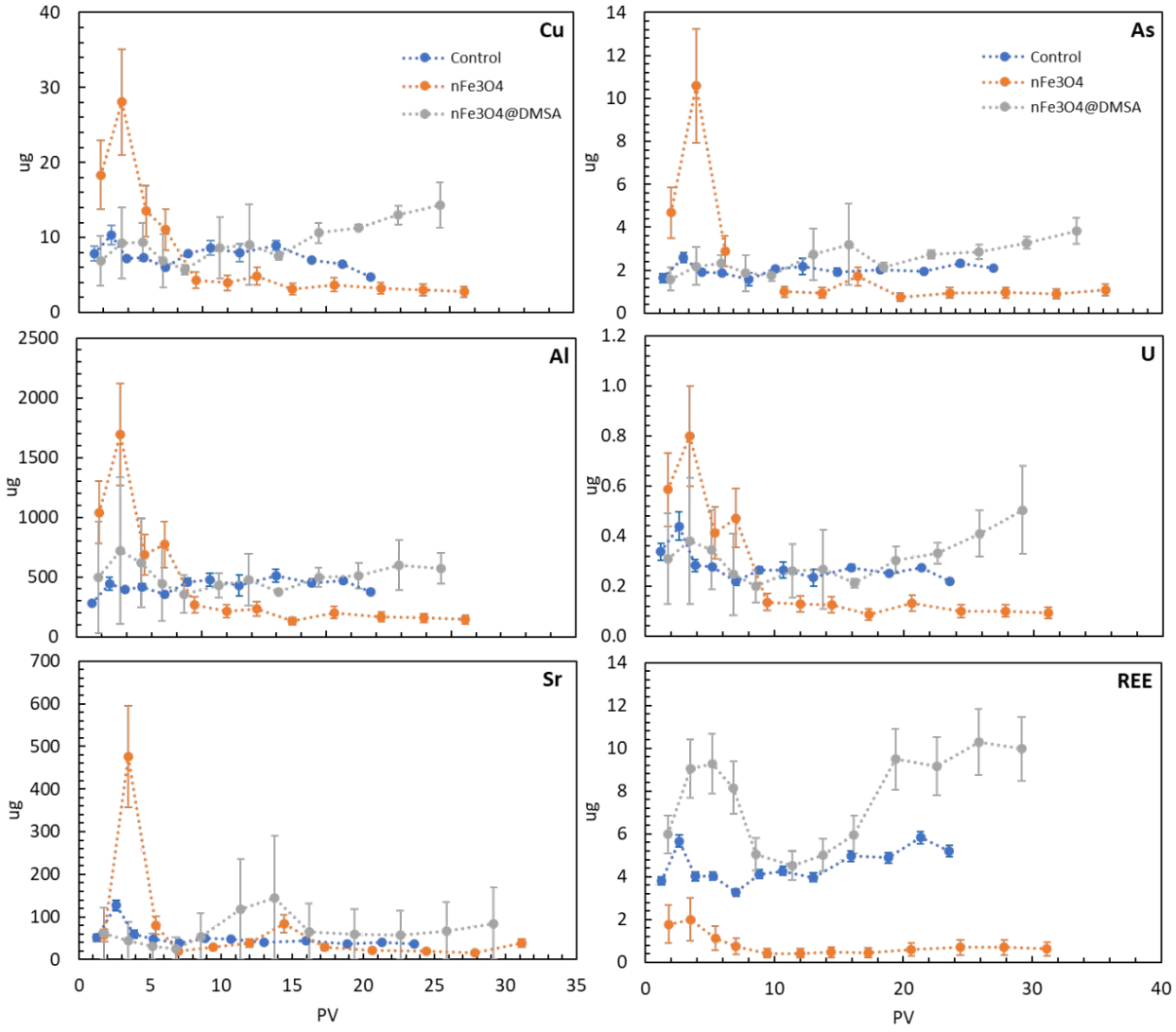

Figure S5. Mass leached < 200 nm of copper (cu), Arsenic (As), Aluminum (Al), Uranium (U), Strontium (Sr) and Rare Earth Elements (REE) during each leaching.

Table S1. Magnetite AMS sheet from Haavik C, Stolen S, Fjellvag H, Hanfland M, Hausermann D, American Mineralogist 85 (2000) 514-523, Equation of state of magnetite and its high-pressure modification: Thermodynamics of the Fe-O system at high pressure (database: # amcsd 0002411). http://serc.carleton.edu/

2-THETA	INTENSITY	D-SPACING	H	K	L	Multiplicity
18.77	8.68	4.728	1	1	1	8
30.88	28.49	2.8953	2	2	0	12
36.39	100	2.4691	3	1	1	24
38.07	8.6	2.364	2	2	2	8
44.24	**19.65**	**2.0473**	**4**	**0**	**0**	**6**
54.93	9.09	1.6716	4	2	2	24
58.57	5.95	1.576	3	3	3	8
58.57	24.11	1.576	5	1	1	24
64.35	38.84	1.4476	4	4	0	12
73.08	3.19	1.2948	6	2	0	24
76.24	8.1	1.2488	5	3	3	24
77.28	3.87	1.2346	6	2	2	24
81.42	2.41	1.182	4	4	4	8
89.57	3.51	1.0943	6	4	2	48
18.77	8.68	4.728	1	1	1	8
30.88	28.49	2.8953	2	2	0	12

Cell parameters: 8.1891; 8.1891; 8.1891; 90.000; 90.000; 90.000; Space group: Fd3m; X-ray wavelength: 1.541838; MAX. ABS. Intensity / Volume**2: 97.1243910

Table S 2. Trace elements analysis on nano-F_3O_4 uncoated and coated

	Uncoated	Coated		Uncoated	Coated
	µg L^{-1}			µg L^{-1}	
Li	0.01	0.00	La	0.007	0.01
Be	0.00	0.00	Ce	0.0007	0.00
B	0.46	0.00	Pr	3.8×10^{-5}	0.00
Mg	0.73	3.92	Nd	0.0005	0.00
Al	1.22	10.66	Sm	9.3×10^{-5}	0.00
K	12.00	0.00	Eu	0.0003	0.00
Ca	3.75	18.07	Gd	<LD	0.00
Sc	0.01	0.00	Tb	9.4×10^{-5}	0.00
V	0.00	0.02	Dy	<LD	0.00
Cr	0.37	1.35	Ho	<LD	0.00
Mn	4.09	15.39	Er	<LD	0.00
Co	0.12	0.45	Tm	2.9×10^{-6}	0.00
Ni	2.84	5.50	Yb	1.7×10^{-5}	0.00
Cu	0.88	2.64	Lu	<LD	0.00
Zn	0.31	2.45	Pb	0.07	0.07
Ga	0.00	0.02	Th	0.007	0.01
As	0.00	0.10	U	6.2×10^{-5}	0.00
Rb	0.01	0.00			
Sr	0.04	0.31			
Y	0.00	0.01			
Cd	0.00	0.01			
Sb	0.01	0.03			
Ba	0.06	0.26			

Table S3. Key properties of soil grain size mixtures A

Soil fraction	*Air dry moisture (%)*	*SOM (%)*	*CEC (meq/100 g)*	*pH_{soil}*	*Nitrogen (g/kg)*	*C/N*	*Sand (%)*	*Silt (%)*	*Clay (%)*
A	3.2	8.5	20.4	5.0	4.5	11	9.9	69.2	20.9

Table S 4. Element analysis of the soil fraction A.

Element	*ppm*	*Element*	*ppm*	*Element*	*%*
As	7.3	**Nb**	10.5	**SiO_2**	61.5
Ba	406.3	**Nd**	24.7	**Al_2O_3**	11.6
Be	1.7	**Ni**	32.0	**Fe_2O_3**	3.6
Bi	0.2	**Pb**	23.2	**MnO**	0.04
Cd	0.3	**Pr**	6.1	**MgO**	0.9
Ce	55.4	**Rb**	66.8	**CaO**	0.5
Co	9.5	**Sc**	11.8	**Na_2O**	0.9
Cr	82.8	**Sb**	0.9	**K_2O**	1.8
Cs	4.3	**Sm**	5.0	**TiO_2**	0.7
Cu	21.0	**Sn**	3.0	**P_2O_5**	0.2
Dy	4.3	**Sr**	59.3	**PF**	18.0
Er	2.5	**Ta**	0.9	**Total**	99.6
Eu	1.0	**Tb**	0.7		
Ga	14.8	**Th**	7.8		
Gd	4.4	**Tm**	0.4		
Ge	1.4	**U**	2.7		
Hf	6.8	**V**	77.5		
Ho	0.9	**W**	1.6		
In	**< L.D.**	**Y**	24.1		
La	26.1	**Yb**	2.6		
Lu	0.4	**Zn**	76.3		
Mo	0.7	**Zr**	269.9		

Table S5. Initial composition of the leaching solution for three exposures and the triplicates. L.D is limit of detection.

	Leaching solution				*Column parameters*						
# ID	C_{org}	Fe	pH	T	d	Flow rate	PV	m_{soil}	H	Fe_2O_3	Fe
	(mg L^{-1})	(mg L^{-1})		°C	(g cm^{-1})	(mL min^{-1})	mL	g	cm	g	
Blank a	0.06	<L.D.	6.5	20	0.58	5.21 ± 0.3	300	275	37.5	9.9	3.5
Blank b	0.03	<L.D.	6.5	20	0.61	5.25 ± 0.4	294	292.6	38	10.5	3.7
Blank c	0.02	<L.D.	6.5	20	0.59	5.09 ±0.2	284	276.9	37.5	10.0	3.5
nFe_3O_4 a	0.21	39.8±1.2	6.5	20	0.6	5.17 ± 0.5	295	285.9	38	10.3	3.6
nFe_3O_4 b	0.18	41.1±0.9	6.5	20	0.59	5.42 ± 0.3	294	281.3	38	10.1	3.5
nFe_3O_4 c	0.23	38.6±0.7	6.5	20	0.61	5.07 ± 0.3	324	290.4	38	10.5	3.7
nFe_3O_4@DMSA a	305.7	41.3±0.8	6.5	20	0.57	5.4 ± 0.2	308	270	38	9.7	3.4
nFe_3O_4@DMSA b	287.9	38.9±1.1	6.5	20	0.56	5.8 ± 0.5	300	268	38	9.6	3.4
nFe_3O_4@DMSA c	300.5	40.6±1.0	6.5	20	0.54	5.2 ± 0.3	320	258	38	9.3	3.2

Table S6. Total amount of dissolved organic carbon and iron < 220nm during the soil leaching experiments.

Avg	*PV*	*s.d.*	*DOC (mg)*	*s.d.*	*Fe (ug)*	*s.d.*
Control-S1	1.2	0.078	131.3	11.5	468.0	46.2
Control-S2	2.6	0.202	174.6	28.4	566.5	65.4
Control-S3	3.9	0.222	92.5	11.6	499.5	1.8
Control-S4	5.2	0.189	81.2	14.6	561.6	34.7
Control-S5	7.0	0.280	62.1	4.7	440.0	14.0
Control-S6	8.8	0.437	74.2	6.2	554.3	38.2
Control-S7	10.7	0.549	69.1	8.7	493.9	64.3
Control-S8	13.0	0.611	54.4	6.7	315.9	32.2
Control-S9	15.9	0.688	65.6	4.2	291.8	16.5
Control-S10	18.8	0.764	61.2	7.8	295.0	26.2
Control-S11	21.3	0.869	68.7	5.5	412.5	34.8
Control-S12	23.5	0.962	57.5	2.9	456.3	32.4
Total			**992.5**	**113.1**	**5355.3**	**406.7**
nFe_3O_4-S1	1.8	0.09	138.72	56.07	694.42	166.88
nFe_3O_4-S2	3.5	0.07	97.22	13.82	1182.35	372.96
nFe_3O_4-S3	5.4	0.37	62.47	20.35	668.31	271.27
nFe_3O_4-S4	7.0	0.22	34.52	2.25	357.37	41.26
nFe_3O_4-S5	9.4	0.24	30.48	4.55	174.15	50.78
nFe_3O_4-S6	12.0	0.21	22.45	1.43	110.14	2.09
nFe_3O_4-S7	14.4	0.49	18.83	0.49	112.09	16.99
nFe_3O_4-S8	17.3	0.41	20.71	4.11	89.19	50.32
nFe_3O_4-S9	20.6	0.50	24.37	0.87	79.02	27.78
nFe_3O_4-S10	24.4	0.83	30.42	5.06	93.44	37.32
nFe_3O_4-S11	27.8	0.83	29.22	2.57	120.30	9.35
nFe_3O_4-S12	31.1	0.72	27.07	1.68	161.87	23.22
Total			**536.5**	**113.2**	**3842.6**	**1070.2**
nFe_3O_4@DMSA-S1	1.7	0.05	160.3	21.2	1228.7	151.2
nFe_3O_4@DMSA-S2	3.5	0.10	242.4	54.5	2836.1	526.5
nFe_3O_4@DMSA-S3	5.1	0.07	259.7	78.5	4177.7	512.8
nFe_3O_4@DMSA-S4	6.8	0.14	257.8	81.9	3541.2	605.3
nFe_3O_4@DMSA-S5	8.6	0.20	193.7	62.4	1681.1	180.3
nFe_3O_4@DMSA-S6	11.4	0.46	104.4	29.3	884.2	173.2
nFe_3O_4@DMSA-S7	13.8	0.49	46.9	12.5	874.4	241.9
nFe_3O_4@DMSA-S8	16.2	0.55	56.9	13.4	998.1	334.9
nFe_3O_4@DMSA-S9	19.4	0.75	84.9	15.1	1088.6	388.3
nFe_3O_4@DMSA-S10	22.6	0.95	105.6	19.2	1130.6	419.4
nFe_3O_4@DMSA-S11	25.8	1.09	104.4	25.6	1316.1	505.9
nFe_3O_4@DMSA-S12	29.2	1.3	131.0	36.0	1274.5	487.8
Total			**1748.0**	**449.5**	**21031.3**	**4527.6**

Analysis 1 SUVA and Aromaticity treatment

A normalized parameter of specific ultraviolet absorbance (SUVA), which is calculated as the ratio between the UVA at a given wavelength and the organic carbon content, has been applied in water chemistry (Traina et al., 1990; Weishaar et al., 2003).

Thus, absorbance at 254 nm was measured to obtained SUVA (specific ultra-violet absorbance, eq. 1) values in according to:

$$SUVA = \frac{A_{254nm}}{[OC]}$$

The values of SUVA determined at 254 nm can be used to describe the composition of water in terms of hydrophobicity and hydrophilicity, and $SUVA_{254} > 4$ L mg^{-1} m^{-1} indicates mainly hydrophobic and especially aromatic material, whereas $SUVA_{254} < 3$ L mg^{-1} m^{-1} represents hydrophilic material (Edzwald et al., 1985).

The values of $SUVA_{254}$ were found to be strongly correlated with percent aromaticity for organic matter isolated from aquatic environment (Weishaar et al., 2003) in according to:

$$Aromaticity = 6.52 \times SUVA + 3.63$$

These parameters were used such as an indicator of the chemical composition of the leached NOM.

Analysis 2 Procedure and data treatment for Py-GCMS analysis

Approximately 2 mg of solid residue (lyophilizate) were introduced into an 80 µL aluminum reactor with an excess of solid tetramethylammonium hydroxide (TMAH – ca. 10 mg). The THM reaction was performed on-line using a vertical micro-furnace pyrolyser PZ-2020D (Frontier Laboratories, Japan) operating at 400°C during 1 min. The products of this reaction were injected into a gas chromatograph (GC) GC-2010 (Shimadzu, Japan) equipped with a SLB 5MS capillary column (60 m × 0.25 mm ID, 0.25 µm film thickness) in the split mode. The split ratio was adapted according to the sample and ranged from 10 to 30. The temperature of the transfer line was 321°C and the temperature of the injection port was 310°C. The oven temperature was programmed from an initial temperature of 50°C (held for 2 min) rising to 150°C at 7°C/min, then rising from 150°C to 310°C (held for 20 min) at 4°C/min. Helium was used as the carrier gas, with a flow rate of 1.0 ml/min. Compounds were detected using a QP2010+ mass spectrometer (MS) (Shimadzu, Japan) operating in the full scan mode. The temperature of the transfer line was set at 280°C, and molecules were ionized by electron impact using energy of 70 eV. The temperature of the ionization source was set at 200°C. The list of analyzed compounds and m/z ratios used for their integration are given in the supplementary materials (Table S1). Compounds were identified on the basis of their full-scan mass spectra by comparison with the NIST library and with published data. They were classified into three categories: lignin (LIG) and tannin (TAN) markers, carbohydrates (CAR) and fatty acids (FA). The peak area of the selected m/z for each compound was integrated and corrected by a mass spectra factor (MSF) calculated as the reciprocal of the proportion of the fragment (used for the integration) relating to the entire fragmentogram provided by the NIST library.

LIG were quantified using an internal calibration for 3,4-dimethoxybenzoic acid methyl ester, 3-(4-methoxyphenyl)-prop-2-enoic acid, methyl ester and 3,4,5-trimethoxybenzoic acid methyl ester. Dihydrocinnamic acid d9 methyl ester (CDN Isotopes, D5666) was used as an internal standard and was added to the system prior to the THM step (10µL of a 25 ppm solution in methanol). The other LIG and TAN compounds were quantified by assuming that their quantification factors were similar to those of 3,4-dimethoxybenzoic acid methyl ester. For this type of analysis, the relative standard deviation (RSD) represents approximately 10% of the values.

The proportion of each compound class was calculated by dividing the sum of the areas of the compounds in this class by the sum of the peak areas of all analyzed compounds multiplied by 100 in order to express it as a percentage. The use of THM-GC-MS to investigate the temporal variability of the DOM composition meant that it was necessary to assume that the ionization efficiency and matrix effects are equivalent for all analyzed compounds in all samples.

Treatment of molecular data

The classification of molecular markers generated by THM-GC-MS into microbial and plant-derived markers has been performed according to Jeanneau et al. (2014). Briefly, the analyzed compounds were classified as follows. LIG-TAN are characteristic of DOM inherited from plant-derived inputs, whereas CAR and FA can be inherited from both plant-derived and microbial sources. The proportion of microbial CAR was calculated using an end-member mixing approach (EMMA) based on the deoxyC6/C5 ratio, assuming that it is 0.5 and 2.0 for plant-derived and microbial inputs, respectively (Rumpel and Dignac, 2006). C6 were not considered since they can derive from the THM of cellulose leading to an increase of the plant-derived C6 signal. The proportion of microbial FA was calculated as the % low molecular weight FA (< C19) by excluding C16:0 and C18:0 that can be inherited from plant-derived or microbial inputs. The microbial FA were composed of C12:0, C13:0, C14:0, C15:0, C17:0, anteiso and iso C15:0 and C17:0, iso C16:0, C16:1 and C18:1 commonly used as bacterial indicators (Frostegård et al., 1993). The proportion of microbial markers was calculated as the sum of the proportion of microbial CAR multiplied by the proportion of CAR plus the proportion of microbial FA multiplied by the proportion of FA. From this value, it is possible to calculate the proportion of plant-derived markers among the analyzed compounds. For this calculation, it is assumed that the modification of the distribution of CAR and FA would only be due to the relative proportion between these plant-derived and microbial inputs. Although these assumptions still need to be validated by investigating pure and known mixtures of vegetal and microbial sources, this approach can be used to approximate the proportions of plant-derived and microbial CAR.

K. Bourikas, J. Vakros, C. Kordulis and A. Lycourghiotis, 2003. Potentiometric Mass Titrations: Experimental and Theoretical Establishment of a New Technique for Determining the Point of Zero Charge (PZC) of Metal (Hydr)Oxides. Journal of Physical Chemistry B, 107, 9441–9451.

Edzwald, J.K., Becker, W.C., Wattier, K.L., 1985. Surrogate Parameters for Monitoring Organic Matter and THM Precursors. Journal (American Water Works Association) 77, 122-132.

Frostegård, Å., Tunlid, A., Bååth, E., 1993. Phospholipid Fatty Acid Composition, Biomass, and Activity of Microbial Communities from Two Soil Types Experimentally Exposed to Different Heavy Metals. Applied and Environmental Microbiology 59, 3605-3617.

Jeanneau, L., Jaffrezic, A., Pierson-Wickmann, A.-C., Gruau, G., Lambert, T., Petitjean, P., 2014. Constraints on the Sources and Production Mechanisms of Dissolved Organic Matter in Soils from Molecular Biomarkers. Vadose Zone Journal 13.

Rumpel, C., Dignac, M.-F., 2006. Gas chromatographic analysis of monosaccharides in a forest soil profile: Analysis by gas chromatography after trifluoroacetic acid hydrolysis and reduction–acetylation. Soil Biology and Biochemistry 38, 1478-1481.

Stevenson, F.J., 1982. Humus Chemistry. Genesis, Composition, Reactions., New York.

Tam, S.C., Sposito, G., 1993. Fluorescence spectroscopy of aqueous pine litter extracts: effects of humification and aluminium complexation. Journal of Soil Science 44, 513-524.

Traina, S.J., Novak, J., Smeck, N.E., 1990. An Ultraviolet Absorbance Method of Estimating the Percent Aromatic Carbon Content of Humic Acids. Journal of Environmental Quality 19, 151-153.

Weishaar, J.L., Aiken, G.R., Bergamaschi, B.A., Fram, M.S., Fujii, R., Mopper, K., 2003. Evaluation of Specific Ultraviolet Absorbance as an Indicator of the Chemical Composition and Reactivity of Dissolved Organic Carbon. Environmental Science & Technology 37, 4702-4708.

Zsolnay, A., Baigar, E., Jimenez, M., Steinweg, B., Saccomandi, F., 1999. Differentiating with fluorescence spectroscopy the sources of dissolved organic matter in soils subjected to drying. Chemosphere 38, 45-50.